

## MODELS OF VARIABILITY IN BLAZAR JETS

A. MASTICHIADIS<sup>1</sup>, J.G. KIRK<sup>2</sup><sup>1</sup>PHYSICS DEPARTMENT, UNIVERSITY OF ATHENS  
GR-15784 Zografos, Athens, Greece<sup>2</sup>MAX-PLANCK-INSTITUT FÜR KERNPHYSIK  
Postfach 10 39 80, D-69029 Heidelberg, Germany**Abstract**

We present the expected variability features in the context of the Synchro-Self-Compton (SSC) model of emission from Active Galactic Nuclei (AGNs). We show that the homogeneous SSC model can describe well the observed multiwavelength spectrum and variability of objects such as Mkn 421 and Mkn 501; however in order to explain the very fast flaring timescales occasionally observed from these objects one should use a laminar, rather than spherical, source geometry. This picture leads naturally to a shock-in-jet model which we approach as a site of diffusive particle acceleration. We show that this acceleration scheme can explain certain characteristic features of AGN X-ray spectra and can provide us with further observational tests.

## 1 Introduction

During the last decade there has been a drastic change in our picture of high energy emission from Active Galactic Nuclei (AGNs). The 2nd CGRO catalogue lists over 40 AGNs as strong sources of GeV gamma rays (Thompson et al 1995) while two AGNs,

Mkn 421 and Mkn 501, have been detected in the TeV regime (Punch et al. 1992, Quinn et al. 1996). All of these AGNs belong to the category of blazars, which include OVV, flat radio sources, many of which exhibit superluminal motion. The fact that up to date not a single radio quiet AGN has been detected in the GeV/TeV regime (Lin et al. 1992) has put a first strong constraint on the theories of gamma-ray emission from AGNs, while, at the same time, has given arguments in favour of certain theories for AGN unification (Urry & Padovani 1995).

On the theoretical front it became quickly apparent that the gamma-ray emission was connected with processes in the jet rather than in the core. While this general picture remains more or less undisputed, many models have been proposed for the high energy emission itself; these can be roughly divided in leptonic or hadronic in origin, depending on whether it is electrons or protons which are responsible for the gamma-ray emission. Thus while there are models which invoke protons as the ultimate source of high energy emission (Mannheim 1993, Bednarek & Protheroe 1997a), the majority of the proposed models assume that the gamma-rays come from inverse Compton scattering of relativistic electrons on some soft photon targets. The source of these targets is still an open question and many possible origins have been proposed such as accretion disk photons (Dermer, Schlickeiser & Mastichiadis 1992), diffuse isotropic photons coming from regions such as the broad line clouds (Sikora, Begelman & Rees 1994), internally produced synchrotron photons (Maraschi, Ghisellini & Celotti et al. 1992; Marscher & Travis 1996, Inoue & Takahara 1996) or combinations thereof (Dermer, Sturner, Schlickeiser 1997) with each model giving rather similar spectral features and characteristics.

A very interesting aspect which emerged from the intense gamma-ray monitoring of the sources was the discovery of fast variability. So in addition to the already known variability in the X-ray regime, Mkn 421 was discovered to exhibit TeV flares, the fastest of which had a duration of about 15 minutes (Gaidos et al. 1996). More powerful sources, such as 3C279, have shown variability in the GeV regime of the order of an hour (Hartman et al. 1996). These observations put new, interesting constraints on the theoretical models of high energy emission from AGNs since one expects the particle cooling times to be of the order of the flare itself. The imposed constraints become even tighter from recent results of multiwavelength campaigns which show certain trends in the evolution of flares along the EM spectrum. Thus Mkn 421 was discovered to exhibit quasisimultaneous variation in the keV and TeV regime (Macomb et al. 1995), while other energy regimes (most notably the GeV regime) remained virtually unaffected. The other AGN detected in TeV, Mkn 501, has shown similar trends (Catanese et al. 1997, Pian et al. 1998).

The aforementioned observations provoked a flurry of models which addressed explicitly either the fast variability (Salvati, Spada & Pacini 1998), the multiwavelength spectrum (Ghisellini, Maraschi & Dondi 1997) or both (Mastichiadis & Kirk 1997). In §2 of the present article we will review the basic features of such models especially in the context of the so-called homogeneous synchrotron self-Compton models (SSC). In §3 we will address explicitly the problem of particle acceleration and we will present a simple way one can explain certain observations with the picture of accelerating/radiating particles.

## 2 Homogeneous Synchrotron-Self Compton Models

### 2.1 Spherical Models

This class of models, based on the ideas first put forward by Jones, O'Dell & Stein (1974), has extensively been discussed elsewhere (Kirk & Mastichiadis 1997, Mastichiadis & Kirk 1997–henceforth MK97, and Ghisellini, Maraschi & Dondi 1997), however for the sake of completeness we give a brief overview here. As the above authors have shown, a homogeneous region containing magnetic fields and relativistic electrons can reproduce the observed spectrum of the blazar Mkn 421 whilst allowing for time variations on the scale of roughly 1 day. In order to address explicitly the temporal behaviour of the spectrum, MK97 used a set of time-dependent, spatially averaged kinetic equations for the electrons and photons adopting the approach outlined in Mastichiadis & Kirk (1995). The electrons are assumed to have a power-law uniform injection in a spherical source (blob) of radius  $R$ ; the blob itself is supposed to move at some small angle  $\theta$  to our line of sight with a bulk Lorentz factor  $\Gamma$ . The electrons lose energy from synchrotron radiation on a magnetic field of strength  $B$  and from inverse Compton radiation on the produced synchrotron photons. The so obtained electron distribution function is then convolved with the single electron synchrotron and inverse Compton emissivities and the overall photon spectrum is obtained after allowing for the possibility of photon-photon pair production –a process which turns out to be negligible for the parameters used.

Seven independent parameters are needed to determine a stationary spectrum in this model. They are the Doppler-boosting factor  $\delta = [\Gamma(1 - B_b \cos \theta)]^{-1}$  (with  $B_b$  the bulk velocity of the source), the size of the source  $R$ , its magnetic field  $B$ , the mean time during which particles are confined in the source  $t_{\text{esc}}$ , and three parameters determining the injected relativistic electron distribution: its luminosity, or compactness  $\ell_e$ , the spectral index  $s$  and the maximum Lorentz factor of the electron distribution  $\gamma_{\text{max}}$ . The inclusion of the particle escape time  $t_{\text{esc}}$  becomes necessary from the fact that the photon spectrum is rather flat between the radio and the infra-red region, implying that the radiating particles do not have time to cool significantly. It turns out that this fit leaves a free parameter which can be suitably chosen as either the Doppler factor of the blob  $\delta$  or the timescale over which variability can be observed  $t_{\text{var}}$  (in sec). These two quantities are related by the scaling relation  $\delta = 267t_{\text{var}}^{-1/4}$  ( $t_{\text{var}}$  expressed in sec). For the reported variability of about one day ( $t_{\text{var}} = 10^5$  sec–Macomb et al 1995) one readily finds  $\delta = 15$ , which is close to the usually assumed values of the Doppler factor. The spectrum of the flare can be fitted in a time-dependent fashion (i.e. before complete cooling can be achieved) by changing  $\gamma_{\text{max}}$  by a factor of a few (MK97).

### 2.2 Slab models

Recently, very rapid variations in the TeV flux of Mkn 421 have been reported (Gaidos et al 1996). As it was stated above, in the framework of the homogeneous SSC spherical models this implies that acceptable fits can be found only by increasing the Doppler factor  $\delta$ . Thus, as the above scaling formula between  $\delta$  and  $t_{\text{var}}$  suggests, a choice of  $t_{\text{var}} = 1000$  sec (so as to agree with the observed flare timescale) would mean  $\delta$  of

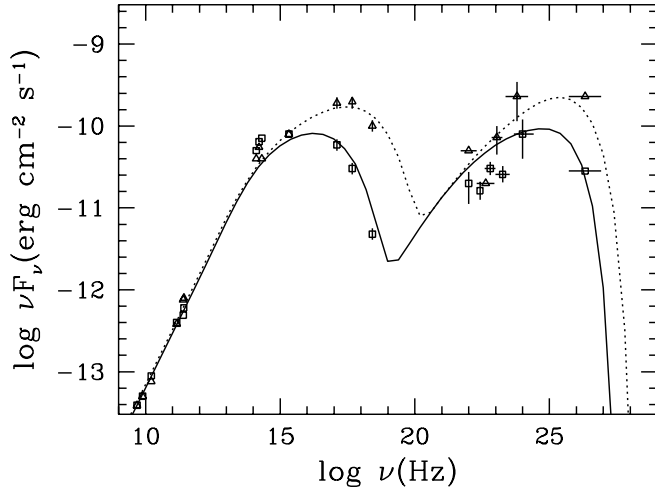


Figure 1: Low and high states of the multiwavelength spectrum of Mkn421. The data points were taken from Macomb et al (1996). The fits were made using a laminar geometry for the emitting region. For the parameters used see text.

the order of 50, a value which is above those indicated by observations of apparent superluminal motion (Vermeulen & Cohen 1994).

An alternative way of approach can be understood as follows: Assuming that the electrons cool due to synchrotron radiation and that their cooling time  $t_{c,3}$  is given in units of  $10^3$  sec we can write  $t_{c,3} \simeq 10^6 \gamma^{-1} B^{-2} \delta^{-1}$  sec where  $\gamma$  is the Lorentz factor of the particle in the rest frame of the emitting plasma and  $B$  is the magnetic field in gauss. The highest energy photons (in units of 10 keV) emitted by these particles are  $\nu_{10} \simeq 10^{-12} \gamma^2 B \delta$ . These relations imply  $B \simeq 1 t_{c,3}^{-2/3} \nu_{10}^{-1/3} \delta^{-1/3}$  gauss and  $\gamma \simeq 10^6 t_{c,3}^{1/3} \nu_{10}^{2/3} \delta^{-1/3}$ . Therefore the maximum photon energy radiated by such electrons is  $\nu_{\max} \simeq .5 t_{c,3}^{1/3} \nu_{10}^{2/3} \delta^{2/3}$  TeV. Assuming furthermore that the source has equal amounts of energies in magnetic fields and photons (as seems to be implied by the source's equal amounts of luminosities in the radio to X-ray and soft to very high energy gamma-rays regimes), we obtain an expression for the aspect ratio of the source region  $\eta = d/R$  where  $d = 3 \cdot 10^{13} \delta t_{c,3}$  cm is a thickness measured in the rest frame of the source and  $R$  is defined such that  $\pi R^2$  is the area of the source when projected onto the plane of the sky.

Fig.1 shows a fit to the multiwavelength spectrum of Mkn 421 as this was given in Macomb (1995, 1996). A fit to the same data can be obtained as well by assuming a spherical source but with either a long variability timescale  $t_{\text{var}}$  and a 'canonical' Doppler factor  $\delta$  or with a short  $t_{\text{var}}$  and a high  $\delta$  (see MK97). The present fit for the low state was obtained for  $t_{\text{var}} = 500$  s,  $\delta = 20$ ,  $B = 0.4$  G,  $\gamma_{\max} = 1.4 \cdot 10^5$ ,  $s = 1.7$ ,  $\ell_e = 1.5 \cdot 10^{-5}$  and  $t_{\text{esc}} = 50 t_{\text{cr}}$ . The high state was obtained by increasing  $\gamma_{\max}$  by a factor of 4 while leaving the other parameters unchanged. The corresponding values

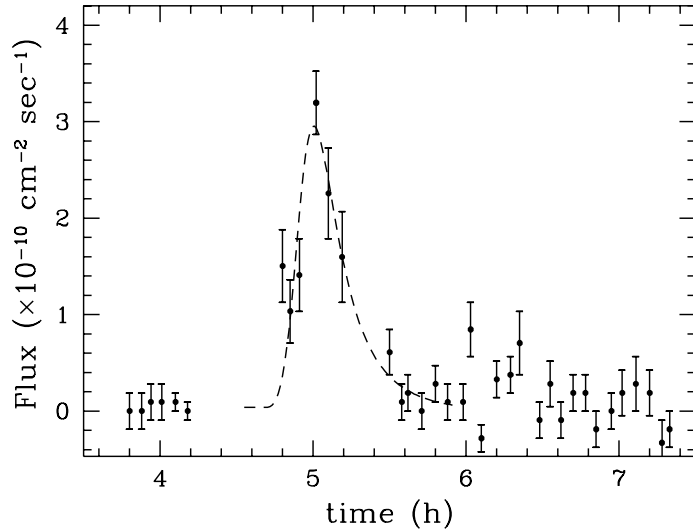


Figure 2: Fit to the flare of Mkn421 observed by Gaidos et al. (1996) for the the parameters used in producing the multiwavelength fit of Figure 1. The flare was obtained by increasing the amplitude of the injected electrons within one crossing time by a factor of 12.

of  $d$  and  $R$  are  $9.2 \cdot 10^{13}$  cm and  $2.8 \cdot 10^{15}$  cm respectively, implying an aspect ratio of  $\eta \simeq .03$ .

As it was pointed in MK97 (and can also be seen from Fig. 1) changes in  $\gamma_{\max}$  result in large variations in the X and TeV regime but these changes are not especially prominent at lower frequencies. An alternative way of producing a flare is to consider an increase in the amplitude  $Q$  of the injected relativistic electrons while leaving the other parameters unchanged. Figure 2 shows the TeV flare produced by increasing  $Q$  by a factor of 12 within one crossing time and consequently decreasing it to its original value. The produced flare can fit quite well the flare reported by Gaidos et al. (1996).

Figure 3 shows the corresponding low and high states of Mkn 501. The parameters used are  $t_{\text{var}} = 500$  s,  $\delta = 15$ ,  $B = 0.5$  G,  $\gamma_{\max} = 1.6 \cdot 10^5$ ,  $s = 1.8$ ,  $\ell_e = .7 \cdot 10^{-5}$  and  $t_{\text{esc}} = 100 t_{\text{cr}}$ . The high state was obtained by increasing  $\gamma_{\max}$  by a factor of 40 (to accommodate the fact that Mkn 501 during one flare in 1997 was observed by OSSE up to energies of 200 keV– Pian et al. 1998). The corresponding values of  $d$  and  $R$  are  $7.1 \cdot 10^{13}$  cm and  $1.1 \cdot 10^{16}$  cm respectively, implying an aspect ratio of  $\eta \simeq .007$ .

From the above it is evident that fast variability can be accommodated in the homogeneous self-Compton models only in the case where the emitting source is a thin structure with a crossing time comparable to the cooling time of the highest energy particles. This can lead naturally to the shock-in-jet model (Marscher & Gear 1985) which we present in the next section.

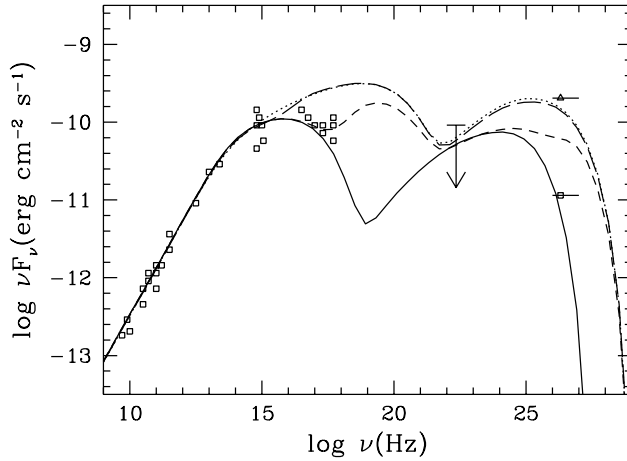


Figure 3: Low and high states of the multiwavelength spectrum of Mkn 501 for a laminar emitting region. Data points were taken from Catanese et al. (1997) and Pian et al.(1998). The short and long dashed lines correspond to the spectrum 3 and  $30 t_{\text{cr}}$  respectively after the change in  $\gamma_{\text{max}}$ . The dotted line corresponds to the new steady-state.

### 3 Particle Acceleration in Blazar Jets

Let us consider a thin shock wave moving down a cylindrically symmetric jet (Marscher & Gear 1985, Kirk, Rieger, & Mastichiadis 1998–henceforth KRM) with a velocity  $u_s$  in the rest frame of the jet. Let also particles be accelerated by the shock through a first order Fermi scheme and subsequently escape downstream where they radiate. Following KRM we will restrict the present analysis only to synchrotron losses and radiation.

The equation that governs the number of particles  $N(\gamma)$  with Lorentz factors between  $\gamma$  and  $\gamma + d\gamma$  in the acceleration zone can be written

$$\frac{\partial N}{\partial t} + \frac{\partial}{\partial \gamma} \left[ \left( \frac{\gamma}{t_{\text{acc}}} - \beta_s \gamma^2 \right) N \right] + \frac{N}{t_{\text{esc}}} = Q \delta(\gamma - \gamma_0) \quad (1)$$

(Kirk, Melrose & Priest 1994), where

$$\beta_s = \frac{4}{3} \frac{\sigma_T}{m_e c^2} \left( \frac{B^2}{8\pi} \right). \quad (2)$$

with  $\sigma_T$  the Thomson cross section. The first term in brackets in the above equation describes acceleration at the rate  $t_{\text{acc}}^{-1}$ , the second describes the rate of energy loss due to synchrotron radiation averaged over pitch-angle (because of the assumed isotropy of the distribution) in a magnetic field  $B$ . Particles are assumed to escape from this region at an energy independent rate  $t_{\text{esc}}^{-1}$ , and to be injected into the acceleration process with a (low) Lorentz factor  $\gamma_0$  at a rate  $Q$  particles per second. Note that the concept

of this ‘acceleration zone’ differs from the emission region in the homogeneous model discussed in the previous section in two important respects: a) particles are injected at low energy and continuously accelerated and b) very little radiation is emitted by a particle whilst in the acceleration zone. A further difference comes from the fact that the high energy cut-off of the electron distribution is given now by a detailed balance between the acceleration and loss rates at the Lorentz factor  $\gamma_{\max} = 1/(\beta_s t_{\text{acc}})$ . The variability features therefore do not depend only on the electron cooling timescale but on the interplay between acceleration and loss timescales. For  $\gamma < \gamma_{\max}$  the acceleration rate exceeds the synchrotron loss rate while for  $\gamma > \gamma_{\max}$  the distribution vanishes.

To describe the kinetic equation in the radiation zone we follow Ball & Kirk (1992) and use a coordinate system at rest in the radiating plasma. The shock front then provides a moving source of electrons, which subsequently suffer energy losses, but are assumed not to be transported in space. The kinetic equation governing the differential density  $dn(x, \gamma, t)$  of particles in the range  $dx, d\gamma$  is then

$$\frac{\partial n}{\partial t} - \frac{\partial}{\partial \gamma} (\beta_s \gamma^2 n) = \frac{N(\gamma, t)}{t_{\text{esc}}} \delta(x - x_s(t)) \quad (3)$$

where  $x_s(t)$  is the position of the shock front at time  $t$ . For a shock which starts to accelerate (and therefore ‘inject’) particles at time  $t = 0$  and position  $x = 0$  and moves at constant speed  $u_s$ , the solution of Eq. (3) for  $\gamma > \gamma_0$  is

$$\begin{aligned} n(x, \gamma, t) = & \frac{a}{u_s t_{\text{esc}} \gamma^2} \\ & \left[ \frac{1}{\gamma} - \beta_s \left( t - \frac{x}{u_s} \right) - \frac{1}{\gamma_{\max}} \right]^{(t_{\text{acc}} - t_{\text{esc}})/t_{\text{esc}}} \\ & \Theta \left[ \gamma_1(x/u_s) - (1/\gamma - \beta_s t + \beta_s x/u_s)^{-1} \right], \end{aligned} \quad (4)$$

where  $\gamma_1(t)$  is given by

$$\gamma_1(t) = \left( \frac{1}{\gamma_{\max}} + \left[ \frac{1}{\gamma_0} - \frac{1}{\gamma_{\max}} \right] e^{-t/t_{\text{acc}}} \right)^{-1}. \quad (5)$$

To obtain the synchrotron emissivity as a function of position, time and frequency we convolve the density  $n$  with the synchrotron Green’s function  $P(\nu, \gamma)$ . At a point  $x = X$  ( $> u_s t$ ) on the symmetry axis of the source at time  $t$  the specific intensity of radiation in the  $\vec{x}$  direction depends on the retarded time  $\bar{t} = t - X/c$  and is given by

$$I(\nu, \bar{t}) = \int d\gamma P(\nu, \gamma) \int dx n(x, \gamma, \bar{t} + x/c) \quad (6)$$

At this point we stress that in this model one needs to integrate the differential electron density over the spatial coordinate since, in contrast to the homogeneous models, the acceleration region is distinct from the cooling region.

### 3.1 Spectral Signatures of Acceleration

As in the case of the homogeneous models we first seek parameters that could fit specific blazar spectra in a steady state and then we try to induce a flare by changing some parameter of the fit.

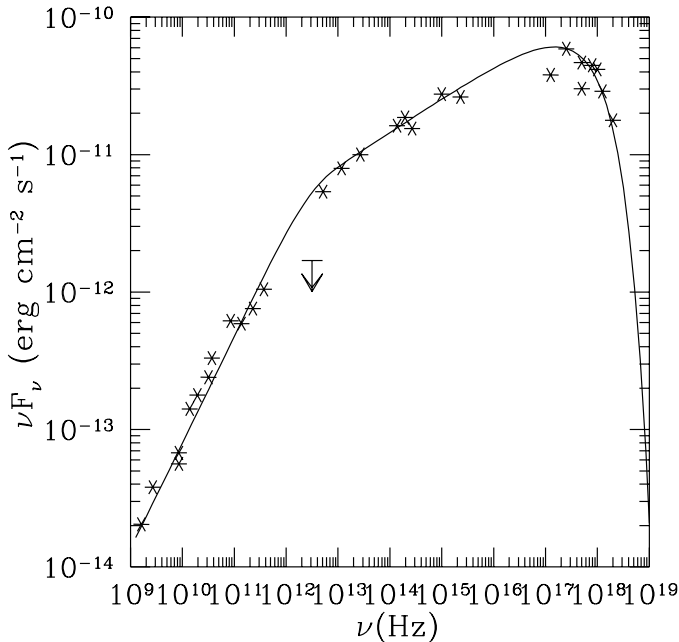


Figure 4: The radio–X-ray spectrum of Mkn 501 as calculated from the acceleration model described in Section 3 once in steady-state. The data were taken from the collation of Catanese et al. 1997.

As an example, we show in Fig. 4 observations of the object Mkn 501. The gamma-ray emission of this object is not included in this figure, since, according to §2, it is not thought to arise as synchrotron radiation. The form of the spectrum is very close to that given by Meisenheimer & Heavens (1987), who used an analytic solution to the stationary diffusion/advection equation, including synchrotron losses. Four free parameters are used to produce this fit:

1. the low frequency spectral index  $\alpha = -0.25$ , which corresponds to taking  $t_{\text{acc}} = t_{\text{esc}}/2$
2. the characteristic synchrotron frequency emitted by an electron of the maximum Lorentz factor as seen in the observers frame (taken to be  $1.3 \times 10^{18}$  Hz)
3. the spatial extent of the emitting region, which determines the position of the spectral break at roughly  $5 \times 10^{12}$  Hz
4. the absolute flux level.

Since we restrict our model to the synchrotron emission of the accelerated particles, it is not possible independently to constrain quantities such as the Doppler boosting factor, or the magnetic field. Similarly, the frequency below which synchrotron self-absorption modifies the optically thin spectrum is not constrained. Nevertheless, this model of the synchrotron emission makes predictions concerning the spectral variability in each of the three characteristic frequency ranges which can be identified in Fig. 4. These ranges are generic features of any synchrotron model, so that the predicted variability can easily be applied to the synchrotron emission of other blazars. They are a) the low frequency region, where the particles have not had time to cool before leaving the source (this is the region with  $\alpha = -0.25$  in Fig. 4, below the break at  $5 \times 10^{12}$  Hz) b) the region between the break and the maximum flux, where the particles have had time to cool, but where the cooling rate is always much slower than the acceleration

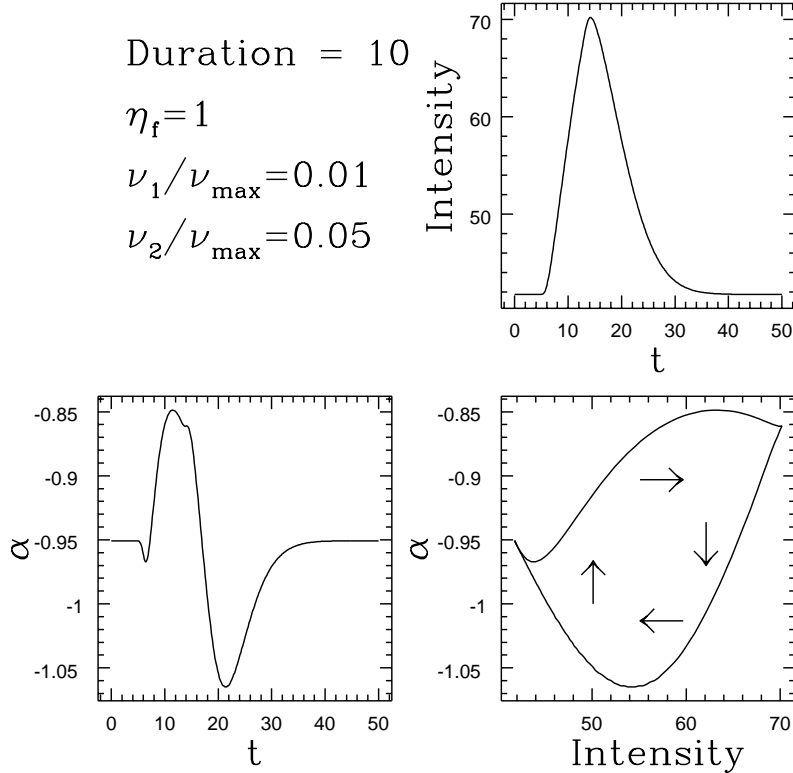


Figure 5: The intensity and spectral index during the flare described by Eq. (8), as a function of time at frequencies away from the high energy cut-off. The loop in the  $\alpha$  vs. intensity plot is followed in the clockwise direction.

rate and the spectrum is close to  $\alpha = -0.75$ , and c) the region around and above the flux maximum at roughly  $10^{17}$  Hz, where the acceleration rate is comparable to the cooling rate.

Variability or flaring behaviour can arise for a number of reasons. When the shock front overruns a region in the jet in which the local plasma density is enhanced, the number of particles picked up and injected into the acceleration process might be expected to increase. In addition, if the density change is associated with a change in the magnetic field strength, the acceleration timescale might also change, and, hence, the maximum frequency of the emitted synchrotron radiation. Considering the case in which the acceleration timescale remains constant, we can compute the emission in a straightforward manner. An increase of the injection rate by a factor  $1 + \eta_f$  for a time  $t_f$  is found by setting

$$Q(t) = Q_0 \quad \text{for } t < 0 \text{ and } t > t_f \quad (7)$$

$$Q(t) = (1 + \eta_f)Q_0 \quad \text{for } 0 < t < t_f \quad (8)$$

Using  $\eta_f = 1$ ,  $t_f = 10t_{\text{acc}}$  and  $u_s = c/10$ , we show the resulting emission at a frequency  $\nu = \nu_{\text{max}}/100$  in Fig. 5. In the case of Mkn 501, this corresponds to a frequency of about  $10^{16}$  Hz, which lies between the infra-red and X-ray regions where the spectral index is close to  $\alpha = -0.75$ . Also shown in this figure is the temporal behaviour of the spectral index, as determined from the ratio of fluxes at  $0.01\nu_{\text{max}}$

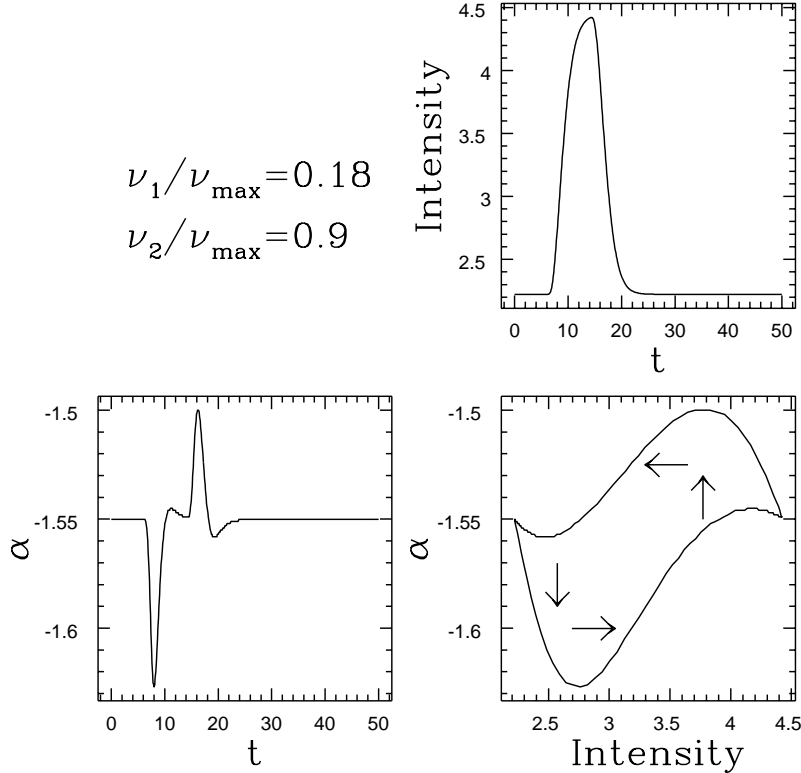


Figure 6: The intensity and spectral index during the flare described by Eq. (8), as a function of time at low frequency. The loop in the  $\alpha$  vs. intensity plot is followed in the anticlockwise direction.

and  $0.05\nu_{\max}$ , through the flare. When plotted against the flux at the lower frequency, the spectral index exhibits a characteristic loop-like pattern, which is tracked in the clockwise sense by the system. This type of behaviour is well-known and has been observed at different wavelengths in several sources e.g. OJ287 (Gear, Robson & Brown 1986), PKS 2155-304 (Sembay et al. 1993) and Mkn 421 (Takahashi et al. 1996). It arises whenever the slope is controlled by synchrotron cooling so that information about injection propagates from high to low energy (Tashiro et al. 1995).

If the system is observed closer to the maximum frequency, where the cooling and acceleration times are equal, the picture changes. Here information about the occurrence of a flare propagates from lower to higher energy, as particles are gradually accelerated into the radiating window. Such behaviour is depicted in Fig.6, where the same flare is shown at frequencies which are an order of magnitude higher than in Fig.5. In the case of Mkn 501, the frequency range is close to  $10^{18}$  Hz. This time the loop is traced anticlockwise. Such behaviour, although not as common, has occasionally been observed in the case of PKS 2155-304 (Sembay et al. 1993).

## 4 Summary

In this paper we have presented a selective account of recent results on AGN variability within the context of a) the homogeneous syncro-self-Compton and b) the diffusive particle acceleration. We have shown that the SSC models give good overall fits to the multiwavelength Mkn 421 and Mkn 501 spectra and can explain the major flares of these objects such as the ones reported by Macomb et al (1995) and Pian et al. (1998) respectively by increasing only one parameter of the fit, namely the high energy cutoff of the injected electron distribution. This type of flare is especially prominent at the high end of the photon distribution, i.e. in the X- and TeV regime, leaving other energy regimes (most notably the GeV gamma-rays) practically unaffected, giving thus an explanation of why EGRET detected neither of these two major outbursts.

The very fast variation of the source Mkn 421, however, as reported by Gaidos et al. (1996) poses a problem for the homogeneous SSC models: in order for the models to satisfy simultaneously i) the high total luminosity, ii) the very fast variability and iii) the transparency to TeV radiation (Bednarek & Protheroe 1997b) one needs either to invoke a high value of the Doppler boosting factor or to abandon the assumptions about a spherical source in favour of a laminar source geometry. As shown above, this new manifestation of the SSC model can provide us with good fits to the AGN observations both in spectral and temporal behaviour (see, for examples, Figures 1-3).

This picture can lead naturally to the shock-in-jet model, i.e. to the picture of a shock advancing down a jet, accelerating, at the same time, particles. Approaching the acceleration by a first order Fermi scheme we have shown that one can get once again remarkably good fits to the multiwavelength spectra of AGN at least from the radio to the X-ray regime (since we have restricted our analysis only to the synchrotron spectra—Fig.4). This approach improves upon the assumptions of homogeneous SSC model, as presented in § 2, mainly by replacing the instantaneous electron injection with the concept of an acceleration timescale. It is therefore the interplay between the acceleration and energy loss timescales that provides us with the different flare behaviours shown in Figures 5 and 6 (for a more examples of this the reader is referred to Kirk, Rieger & Mastichiadis 1999).

## Acknowledgments

AM would like to thank the organisers of the Workshop for their hospitality. This work was supported by the European Commission under the TMR program, contract number FMRX-CT98-0168.

## 5 References

- Ball L.T., Kirk J.G. 1992, ApJ 396, L39
- Bednarek, W., Protheroe, R.J. 1997a, MNRAS 287, L9
- Bednarek, W., Protheroe, R.J. 1997b, MNRAS 292, 646
- Catanese, M. et al. 1997, ApJ 487, L143
- Dermer, C.D., Schlickeiser, R., Mastichiadis, A. 1992, A&A 256, L27
- Dermer, C.D., Sturner, S.J., Schlickeiser, R. 1997, ApJS 109, 103

Gaidos, J.A. et al. 1996, *Nature* 383, 318  
Gear, W.K., Robson, E.I., Brown, L.M.J. 1986, *Nature* 324, 546  
Ghisellini, G., Maraschi, L., Dondi, L. 1996, *A&A Suppl* 120C, 503  
Hartman, R.C. et al. 1996, *ApJ* 461, 698  
Inoue, S., Takahara, F. 1996, *ApJ* 463, 555  
Jones, T.W., O'Dell, S.L., Stein, W.A. 1974, *ApJ* 188, 353  
Kirk, J.G., Mastichiadis, A. 1997, in 'Frontier Objects in Astrophysics and Particle Physics' eds.: F. Giovannelli, G. Mannocchi, Conference Proceedings Vol. 57, page 263 Italian Physical Society (Bologna)  
Kirk, J.G., Melrose, D.B., Priest, E.R. *Plasma astrophysics*, eds. A.O. Benz, T.J.-L. Courvoisier, Springer, Berlin  
Kirk, J.G., Rieger, F.M., Mastichiadis, A. 1998, *A&A* 333, 452 (KRM)  
Kirk, J.G., Rieger, F.M., Mastichiadis, A. 1999, to appear in proceedings of the conference 'BL Lac Phenomenon', eds. L.O. Takalo, A. Sillanpää, Turku 1998  
Lin, Y.C. et al. 1992, *ApJ* 416, L53  
Macomb, D.J. et al. 1995 *ApJ* 449, L99  
Macomb, D.J. et al. 1996 *ApJ* 459, L111 (Erratum)  
Mannheim, K. 1993, *A&A* 269, 67  
Maraschi L., Ghisellini G., Celotti A. 1992, *ApJ* 397, L5  
Marscher, A.P., Gear, W.K. 1985, *ApJ* 298, 114  
Marscher, A.P., Travis, J.P., 1996 *A&A Suppl* 120C, 537  
Mastichiadis A., Kirk, J.G., 1995 *A&A* 295, 613  
Mastichiadis A., Kirk, J.G., 1997 *A&A* 320, 19  
Meisenheimer, K., Heavens, A.F. 1987, *MNRAS* 225, 335  
Pian, E. et al. 1998, *ApJ* 492, L17  
Punch, M. et al. 1992, *Nature* 358, 477  
Quinn, J. et al. 1996, *ApJ* 456, 83  
Salvati, M., Spada, M., Pacini, F. 1998, *ApJ* 495, L19  
Sembay, S. et al. 1993, *ApJ* 404, 112  
Sikora, M., Begelman, M.C., Rees, M.J. 1994, *ApJ* 421, 153  
Takahashi, T. et al. 1996, *ApJ* 470, L89  
Tashiro, M. et al. 1995, *PASJ* 47, 131  
Thompson, D.J. et al. 1995, *ApJS* 101, 259  
Urry, C.M. & Padovani, P. 1995, *PASP* 107, 803  
Vermeulen, R.C. & Cohen, M.H. 1994, *ApJ* 430, 467